Direct observation of defect-mediated cluster nucleation

U. KAISER*[1], D. A. MULLER[2], J. L. GRAZUL[2], A. CHUVILIN[3] AND M. KAWASAKI[4]
[1]Friedrich-Schiller Universität, Jena 07743, Germany
[2]Bell Laboratories, Lucent Technologies, Murray Hill, New Jersey 07974, USA
[3]Boreskov Institute of Catalysis, Novosibirsk 90, 630090 Russia
[4]JEOL USA, Peabody, Massachusetts 01960, USA
*e-mail: kaiser@pinet.uni-jena.de

Published online: 15 September 2002; doi:10.1038/nmat729

Ion implantation is widely used to introduce electrically or optically active dopant atoms into semiconductor devices[1]. At high concentrations, the dopants can cluster and ultimately form deactivating precipitates[2,3], but deliberate nanocrystal formation offers an approach to self-assembled device fabrication. However, there is very little understanding of the early stages of how these precipitates nucleate and grow[1], in no small part because it requires imaging an inhomogenous distribution of defects and dopant atoms buried inside the host material. Here we demonstrate this, and address the long-standing question of whether the cluster nucleation is defect-mediated or spontaneous. Atomic-resolution illustrations are given for the chemically dissimilar cases of erbium and germanium implanted into silicon carbide. Whereas interstitial loops act as nucleation sites in both cases, the evolution of nanocrystals is strikingly different: Erbium is found to gather in lines, planes and finally three-dimensional precipitates, whereas germanium favours compact, three-dimensional structures.

The electronic structure and local site symmetry of isolated impurity atoms can be studied by indirect methods such as photoluminescence, infrared spectroscopy, electron paramagnetic resonance, X-ray spectroscopy and Rutherford backscattering[3–6]. These provide an ensemble average of the dopant properties, which is useful when one or two types of local arrangements dominate. When clustering occurs, the distribution of atoms becomes less homogeneous and the interpretation of these methods becomes more complicated. The later stages of nanocrystal growth can be studied using dark-field, weak-beam or high-resolution transmission electron microscopy (TEM)[7–10]. However, because these methods rely on diffraction or interference contrast, they typically cannot identify buried clusters smaller than 1.5 nm, where the crystal structure is not sufficiently well-defined. Thus, the initial stages of cluster nucleation, which involve only a few dopant atoms, are difficult to study by either class of method. In particular, the question of whether the cluster forms at an existing defect, or can grow spontaneously, could only be studied indirectly—a major problem because this balance is subtle and system-dependent.

However, this growth regime is well-suited for studying with high-angle annular dark-field (HAADF) imaging in a scanning TEM (STEM), which can detect individual impurity atoms with atomic resolution[11]. Here a 200 kV electron beam (in a JEOL 2010F TEM) is focused down to a

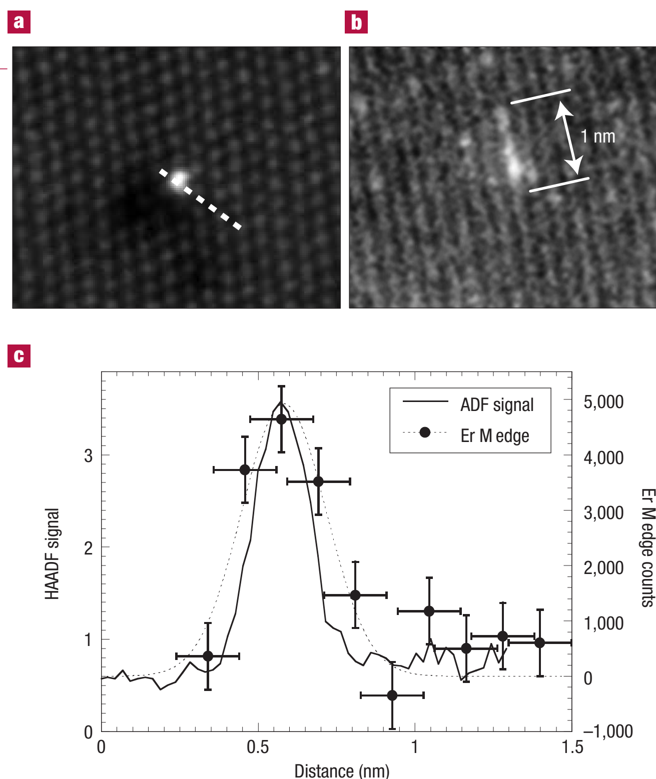

Figure 1 Determining the spatial resolution and sensitivity of the STEM. **a**, HAADF–STEM image of a column, containing 4–5 Er atoms (forming the bright dot), which is viewed end-on when the SiC crystal is oriented along the [11-20] direction. Scale as for **b**. **b**, The same region tilted 30° to [01-10]. The individual Er atoms are not resolved in this projection, but the projected length of 1 nm (giving a 2 nm actual length) and an Er–Er spacing of ~0.5 nm implies that there are about four Er atoms along the line. **c**, Er M edge EELS spectrum obtained along the dashed line in **a**. The HAADF profile shows that the full-width at half-maximum of the probe after scattering is 0.2 nm. The EELS signal takes 10^4 times longer to record, and is blurred by scan instabilities to 0.3 nm. Assuming a peak value of four Er atoms, the uncertainty (indicated by the bars) in the EELS signal is then ± 0.5 atoms.

© 2002 Nature Publishing Group

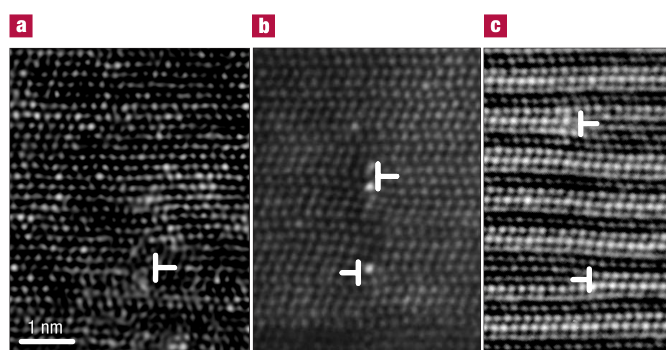

Figure 2 HAADF images of the dislocations (marked by ⊣, the horizontal dash symbolizes the additional SiC monolayer) at the edge of interstitial loops. **a**, Before annealing for 180 s at 1,600 °C. The brighter spots are isolated Er atoms scattered randomly about the matrix—none have yet segregated at the dislocation core. **b**, After annealing, the Er atoms have segregated to the dislocations, and very little remain in the matrix. **c**, Conventional phase-contrast TEM (JEOL 3010) of dislocations after annealing. Unlike HAADF, there is very little contrast from the segregated Er atoms. Scales for **b** and **c** are as for **a**. Further details on the dislocation structure are given in the Supplementary Information.

spot that is less than 0.2 nm in diameter[12], and this is scanned across a section of the implanted crystal that has been thinned down to electron transparency. The transmitted electrons can either be analysed by an on-axis electron-energy-loss spectrometer (EELS), allowing atomic-scale spectroscopy[13–15], or collected by the HAADF detector. The HAADF scattering signal from a single atom is strongly dependent on the atomic number[16–18] (roughly $Z^{1.7}$, hence it is also known as Z-contrast). Therefore, one erbium (Er) atom will appear roughly 62 times brighter than the carbon atom that it is expected to substitute for in SiC, and 15 times brighter than the neighbouring silicon atoms. Contrast from strain fields, although important for detecting light dopant atoms[19,20], produces less than a 10% correction for heavy atoms in the thin samples (8–20 nm thick[11]) used here.

Our interest in SiC stems from its promise as a host material for optically active quantum dots[21], and dopant atoms such as Er (ref. 22), which is of particular interest for telecommunications applications. Further, the size and shape of the nanocrystals can have a profound influence on their optical properties, not only through quantum confinement, but also because of the different electronic structure that a monolayer platelet will have from a point defect or a fully three-dimensional (3D) nanocrystal[21].

Figure 1a shows a HAADF image of a single column of Er atoms in Er-implanted SiC (10^{20} cm^{-3} at 400 keV and 700 °C, ref. 23) that has been annealed for 180 s at 1,600 °C. When the sample is tilted by 30° (Fig. 1b), the length of the Er-decorated column suggests that there are about four

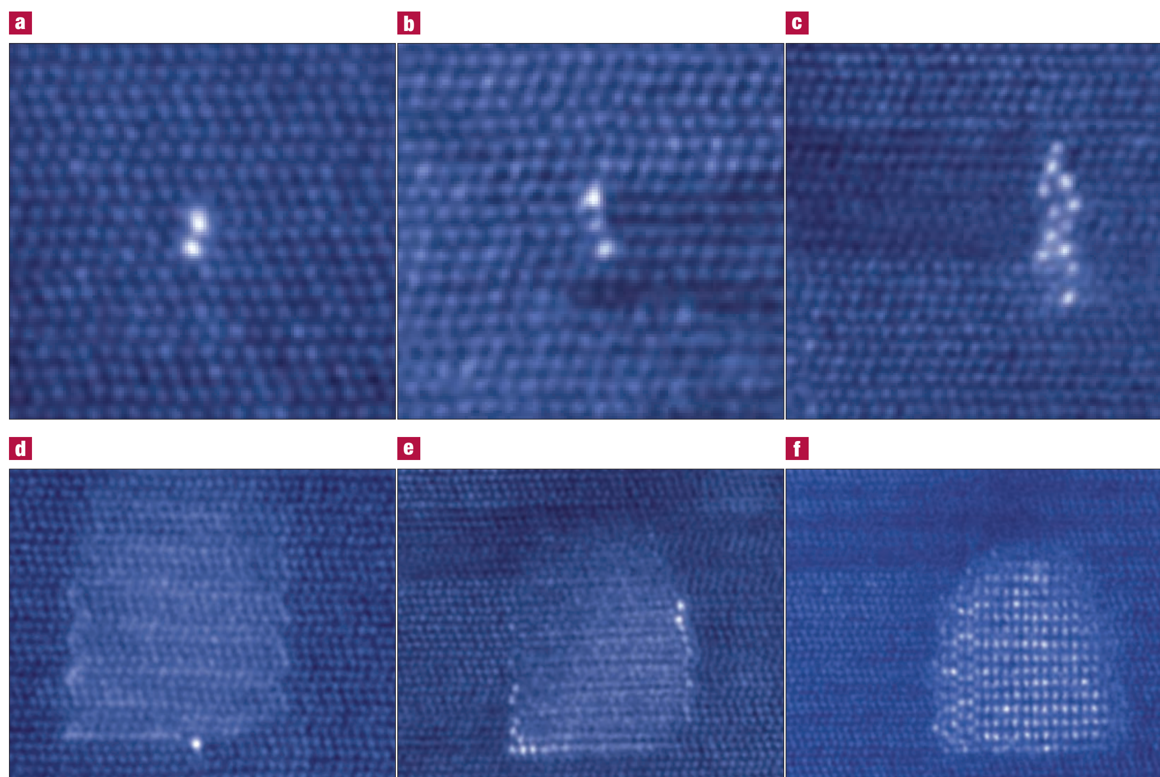

Figure 3 After annealing, HAADF imaging shows that the Er atoms have segregated in precipitates of widely differing sizes. The largest precipitates are still connected to extended defects, whereas the smallest are either no longer associated with defects or in regions with a low initial Er concentration. **a**, **b**, Precipitates composed of two and three columns of Er atoms (with roughly 5–10 atoms in each column). It is likely that these are remnants of interstitial loops that have dissolved. **d**, A 2D Er platelet attached to an Er-rich dislocation core. The platelet is probably not flat (because this would require a line-like profile when edge-on, which has not been seen), but rather when viewed from the side may have an accordion structure similar to that of **c**, which is commonly seen. **e**, This image shows that growth of new layers possibly proceeds from platelet edges, which are decorated first—the extra atoms also have a pattern similar to that of **c**. **f**, A fully 3D unstrained erbium silicide precipitate. The (0001) SiC spacing in the (11-20) lattice images **a**–**f** is 0.252 nm.

© 2002 Nature Publishing Group

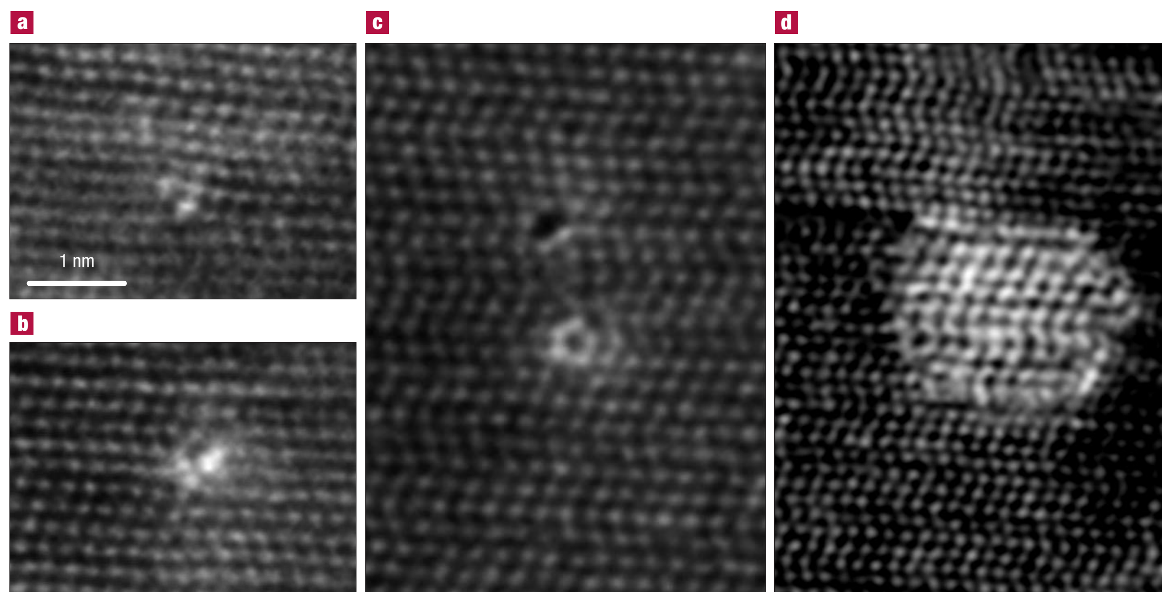

Figure 4 HAADF images showing the different arrangements of Ge atoms (introduced by ion implantation) at dislocation cores and their remnants after annealing for 180 s at 1,600 °C. The arrangement of Ge atoms (brighter dots) around the core is more extended than for Er atoms, but nevertheless, both atoms segregate in the vicinity of the dislocation core (**a–c**). **d**, A precipitate formed at the end of an interstitial loop. The scattering ratio for Ge:Si is 4:1, so single Ge-atom detection is more difficult than for Er atoms. All these clusters are likely to contain more than a single Ge atom in projection. Clusters **b** and **d** were checked independently with Ge-L edge (2p→3d, 4s transition) EELS. Scales for **b**–**d** are as for **a**.

Er atoms present. Figure 1c shows the EELS spectrum for the Er M edge (3d→4f transition), which not only unambiguously certifies that the bright column contains Er, but also demonstrates that EELS from a single column of atoms is possible with 0.3 nm spatial resolution.

During high-dose ion implantation in SiC at elevated temperatures (above 500 °C), and despite the very low rate of self-diffusion for most atoms[24,25], both point and extended defects, such as interstitial loops, can be formed by transient enhanced diffusion[23,26] within the highly disturbed matrix. Because of their extremely low solubility, foreign atoms in SiC have a strong tendency to precipitate. However, the question of whether or not dopant atoms can be trapped by the strain fields of extended defects during implantation has to be considered for each particular ion and implantation condition separately[27], because there are other thermodynamically competitive sites for nucleation. In silicon, for example, it has been suggested that clustering can begin at a single interstitial or vacancy[1,2], and in SiC that interstitial loops form at precipitates, rather than vice versa[8].

In the present study, directly after implantation at elevated temperatures, the specimen showed a high density of small (<20 nm in size) interstitial loops in (0001) planes in the Er-containing region of the SiC matrix, which is located about 100 nm away from the surface. The interstitial loops consist of one SiC plate-like monolayer, analogous to Frank loops in the face-centred-cubic crystals. The edges of the loops are edge dislocations with a Burgers vector of the 1/6<0001> type. The HAADF–STEM image in Fig. 2a shows that the individual Er atoms are randomly distributed throughout the SiC lattice, and that no Er segregation has yet occurred at the core of the edge dislocation at the end of the interstitial loop. In fact no precipitates or nanocrystals can be found anywhere in the sample at this point.

Two striking features are observed after annealing at 1,600 °C: first, the length of the interstitial loops has grown by roughly tenfold, and second, the Er atoms are no longer randomly distributed throughout the lattice but have segregated to the dislocation cores, as shown by the HAADF–STEM image of Fig. 2b. (Because of the high density of the wide loops, edge dislocations bounding neighbouring interstitial loops are often seen in dipole-like configuration). This 1D Er defect seems to be the nucleation site for the nanocrystals, especially as large and growing nanocrystals are still connected to the dislocation loops. Figure 2c shows that it would be extremely difficult to identify or even detect Er at the dislocation core using a conventional phase-contrast TEM image.

Different stages of the nanocrystal formation around dislocation loops can be directly imaged in one specimen, because the local Er atom concentration and diffusion conditions vary with location and depth. Figure 3 provides a snapshot of various clusters after annealing—all are connected to extended defects. The smallest clusters, such as in Fig. 3a, are no longer connected to interstitial loops, however all the large clusters (Fig. 3d–f) usually are. This suggests that the loops are very effective sinks for Er atoms. Further migration of Er atoms to the loop dislocations results in the wetting of a distinct SiC sheet with Er atoms (Fig. 3d). The formation of these 2D Er-containing layers seems to be stimulated by the strong bonding between Er and the matrix Si atoms, because germanium (Ge)-atom clusters of this diameter are already fully 3D. (The 3D structures scatter strongly enough to be detected by conventional TEM, and Kaiser[10] gives examples for Ge.) In Fig. 3e, the formation of 2D clusters parallel to the (10-12) planes are seen around the Er-filled area. These bear close resemblance to the cluster of Fig. 3c that has been expanded along the [10-10] directions.

Further migration of Er atoms leads, at the final stage, to the formation of a new 3D phase (Fig. 3f). These precipitates are now large enough to be identified by traditional electron microscopies, from which they were identified as erbium silicide. The strain fields surrounding the dislocation loop also serve to attract migrating vacancies and interstitials, leading to further growth of the interstitial loops[8], which in turn can capture more Er atoms.

© 2002 Nature Publishing Group

Although the macroscopic influence of dislocations on the transport and precipitation of impurities is well-accepted[1], microscopic evidence of the details is very limited[28]. We cannot generalize too much from the simple structure for Er atoms at the dislocation core: not all atoms segregate in a single column as the Er did. Figure 4 shows a far more complicated arrangement for Ge atoms implanted in SiC. Nevertheless, the Ge atoms have also segregated to the dislocation cores. The platelet structures of Fig. 3c–e are not observed for Ge. Instead, fully 3D clusters are seen (Fig. 4d). These clusters are small enough such that strong quantum confinement effects might be expected[21], and these should be detectable with high-resolution EELS.

Although we expect the balance between surface and volume energies for Er- and Ge-containing clusters to be very different, there are differences even at the earliest stages of nucleation. Figure 4 shows that instead of the compact, single-atom-wide structures seen for Er atoms segregated at dislocation cores, Ge atoms decorate the dislocations in a far more complicated manner. This can probably be rationalized from a ranking of bond strengths in the respective systems, but we are not aware of such calculations, especially for the Er-Si-C system.

Our observations demonstrate that 1D, 2D and 3D Er-atom clusters have been formed after high-dose Er-atom implantation and annealing, and that their location within the hexagonal SiC matrix can be seen directly using HAADF–STEM. Moreover, we imaged the process of Er-atom clusters and nanocrystal formation, and showed that extended matrix defects, and SiC loop dislocations in particular, play an important role, with first the dislocation loops and then the precipitates being formed. This leads to the intriguing possibility that by matching the density of the interstitial loops to the dopant atoms by co-implantation, it should be possible to control the dimensionality, and hence the electronic properties, of the resultant nanocrystals.

Received 17 July 2002; accepted 27 August 2002; published 15 September 2002.

References

1. Fahey, P. M., Griffin, P. B. & Plummer, J. D. Point defects and dopant diffusion in silicon. *Rev. Mod. Phys.* **61**, 289–384 (1989).
2. Fair, R. B. & Weber, G. R. Effect of complex formation on diffusion of arsenic in silicon. *J. Appl. Phys.* **44**, 273–279 (1973).
3. Chadi, D. J. *et al.* Fermi-level pinning defects in highly n-doped silicon. *Phys. Rev. Lett.* **79**, 4834–4837 (1997).
4. Choyke, W. J. & Patrick, L. Photoluminescence of radiation defects in cubic SiC: localized modes and Jahn-Teller effect. *Phys. Rev. B* **4**, 1843–1847 (1971).
5. Greulich-Weber, S. EPR and ENDOR investigations of shallow impurities in SiC polytypes. *Phys. Status Solidi A* **162**, 95–151 (1997).
6. Spitznagel, J. A. *et al.* Ion beam modification of 6H/15R SiC crystals. *Nucl. Instrum. Methods B* **16**, 237–243 (1986).
7. Lhermitte-Sebiret, I., Vicens, J., Chermann, J. L., Levalois, M. & Paumier, E. Transmission electron microscopy and high-resolution electron microscopy studies of structural defects induced in 6H a-SiC single crystals irradiated by swift Xe ions. *Phil. Mag.* **69**, 237–253 (1994).
8. Lebedev, O. L., Van Tendeloo, G., Suvorova, A. A., Usov, I. O. & Suvorov, A. V. HREM study of ion implantation in 6H-SiC at high temperatures. *J. Electron. Microsc.* **46**, 271–279 (1997).
9. Heera, V., Reuther, H., Stoemenos, J. & Pecz, B. Phase formation due to high dose aluminum implantation into silicon carbide. *J. Appl. Phys.* **87**, 78–85 (2000).
10. Kaiser, U. Nanocrystal formation in hexagonal SiC after Ge ion implantation. *J. Electron. Microsc.* **50**, 251–263 (2001).
11. Voyles, P. M., Muller, D. A., Grazul, J. L., Citrin, P. H. & Gossmann, H.-J. L. Atomic-scale imaging of individual dopant atoms and clusters in highly n-type bulk Si. *Nature* **416**, 826–829 (2002).
12. Muller, D. A. & Grazul, J. Optimizing the environment for sub-0.2 nm scanning transmission electron microscopy. *J. Electron. Microsc.* **50**, 219–226 (2001).
13. Batson, P. E. Simultaneous STEM imaging and electron energy-loss spectroscopy with atomic column sensitivity. *Nature* **366**, 727–728 (1993).
14. Browning, N. D., Chisholm, M. M. & Pennycook, S. J. Atomic-resolution chemical analysis using a scanning transmission electron microscope. *Nature* **366**, 143–146 (1993).
15. Muller, D. A. *et al.* The electronic structure at the atomic scale of ultra-thin gate oxides. *Nature* **399**, 758–761 (1999).
16. Loane, R. F., Kirkland, E. J. & Silcox, J. Visibility of single heavy atoms on thin crystalline silicon in simulated annular dark field. *Acta Crystallogr. A* **44**, 912–927 (1988).
17. Howie, A. Image contrast and localized signal selection techniques. *J. Microsc.* **17**, 11–23 (1979).
18. Pennycook, S. J. Z Contrast STEM for materials science. *Ultramicroscopy* **30**, 58–69 (1989).
19. Perovic, D. D., Rossow, C. J. & Howie, A. Imaging elastic strains in high-angle annular dark-field scanning-transmission electron microscopy. *Ultramicroscopy* **52**, 353–359 (1993).
20. Hillyard, S. E. & Silcox, J. Detector geometry, thermal diffuse scattering and strain effects in ADF STEM imaging. *Ultramicroscopy* **58**, 6–17 (1995).
21. Weissker, H. C., Furthmüller, J. & Bechstedt, F. First-principles of optical properties: application to embedded Ge and Si dots. *Phys. Status Solidi B* **224**, 769–773 (2001).
22. Choyke, W. J., Devaty, R. P., Clemen, L. L. & Yoganathan, M. Intense erbium-1.54-μm photoluminescence from 2 to 525 K in ion-implanted 4H, 6H, 15R and 3C SiC. *Appl. Phys. Lett.* **65**, 1668–1670 (1994).
23. Wesch, W., Heft, A., Wendler, E., Bachmann, T. & Glaser, E. High temperature ion implantation of silicon carbide. *Nucl. Instrum. Methods B* **96**, 335–338 (1995).
24. Choyke, W. J., Matsunami, H. & G., P. *Silicon Carbide* (Wiley-VCH, Berlin, 1997).
25. Tairov, Y. M. & Vodakov, Y. A. in *Group IV Materials* (ed. Pankove, J. I.) 35 (Springer, New York, 1977).
26. Usov, I. O., Suvorova, A. A., Sokolov, V. V., Kudryavtsev, Y. A. & Suvorov, A. V. Transient enhanced diffusion of aluminum in SiC during high temperature ion implantation. *J. Appl. Phys.* **86**, 6039–6042 (1999).
27. Skorupa, W., Heera, V., Pacaud, Y. & Weishart, H. Ion beam processing of single crystalline silicon carbide. *Nucl. Instrum. Methods B* **120**, 114–120 (1996).
28. Brown, L. M., Allen, G. & Flewitt, P. Nanochemistry of grain boundaries. *Phys. World* 45–50 (May, 1997).

Acknowledgements

We are grateful to Jim Choyke and Igor Khodos for discussions and Christian Schubert and Gunnar Pasold for ion implantation and annealing. This work has been supported by the German Foundation DFG SFB 196.

Correspondence and requests for material should be addressed to U.K.

Supplementary Information is available on the *Nature Materials* website (http://www.nature.com/naturematerials).

Competing financial interests

The authors declare that they have no competing financial interests.

© 2002 Nature Publishing Group